DOI: 10.19884/j.1672-5220.202509003

Optimization of Multi-Layer Series Micro-Perforated Panels Based on Ant Colony Algorithm

LU Yifan[1*], ZHU Mengke[2], ZHU Congyun[1*], ZHOU Bingtao[1]
1. School of Intelligent Mechatronic Engineering, Zhongyuan University of Technology, Zhengzhou 450007, China
2. Zijin College, Nanjing University of Science and Technology, Nanjing 210046, China

Abstract: To address the increasingly prominent issue of high-frequency traffic noise pollution and to overcome the limitation of narrow sound absorption bandwidth of single-layer micro-perforated panels (MPPs), this study presents a systematic investigation into the sound-absorbing structure of multi-layer series MPPs. First, based on Ma's MPP theory, theoretical sound absorption models for multi-layer structures were derived by using both the acoustic-electrical analogy method and the transfer matrix method. Then, the sound absorption coefficient curves of both methods were compared through COMSOL simulations, confirming the superiority of the transfer matrix method in the analysis of multi-layer structures. Finally, ant colony algorithm (ACA) was introduced to optimize the structural parameters of the multi-layer series MPPs, aiming to broaden the sound absorption bandwidth to match the high-frequency traffic noise spectrum. The results demonstrate that the transfer matrix method outperforms the acoustic-electrical analogy method in predicting the sound absorption characteristics of multi-layer series MPPs. Furthermore, the optimized structure exhibits significantly improved sound absorption performance in the frequency range of 100–4 000 Hz, with MPPs' effectiveness increasing with the number of layers. This study would provide a valuable theoretical foundation and practical design references for broad-frequency traffic noise control.

Keywords: micro-perforated panel (MPP); acoustic-electrical analogy method; transfer matrix method; ant colony algorithm; broad-frequency sound absorption
CLC number: TB535 **Document code**: A
Article ID: 1672-5220(2026)04-0142-11

0 Introduction

Amid rapid economic development, the number of high-frequency noise-emitting transportation vehicles is on the rise, resulting in the growing prominence of high-frequency traffic noise pollution. Academician Ma proposed the micro-perforated panel (MPP) theory[1-2]. However, the traditional single-layer MPP, possessing only one resonant absorption peak, often has a limited sound absorption bandwidth. Many scholars have conducted in-depth research on MPPs based on Ma's theory. Through detailed investigation of two-layer series MPPs, the patterns of resonant frequency, anti-resonance frequency, and corresponding acoustic impedance were studied[3-4]. By synthesizing the sound absorption characteristics under multiple structural parameters, a computational model for the acoustic impedance of two-layer series MPPs was constructed, thereby addressing the narrow frequency bandwidth issue in noise control. However, the effect of the layer number on the sound absorption coefficient is not explored. By studying flexible multi-layer series MPPs sound-absorbing structures, Bravo et al.[5] established a highly efficient sound-absorbing structure. Based on the acoustic-electrical analogy method, Zhao et al.[6] derived the formula for calculating the sound absorption coefficient of three-layer series MPPs and used a genetic algorithm for optimization, to increase the bandwidth. Based on the transfer matrix method, Sheng et al.[7] calculated the sound absorption coefficients of multi-layer series MPPs and employed a genetic algorithm to broaden the absorption bandwidth of four-layer and five-layer series MPPs. The five-layer series MPPs show greater advantages in sound absorption performance. Hu et al.[8] built an acoustic model of two-layer series MPPs by using the acoustic-electrical analogy method and solved for the sound absorption coefficient of three-layer series MPPs by using the transfer matrix method. However, the study only established theoretical models and did not compare their reliability. Based on Ma's theory, Du et al.[9] achieved good agreement between theoretical results for MPP sound absorption coefficients, which were calculated by the transfer admittance method, and COMSOL finite element simulation experiments, thus enhancing the reliability of the theoretical calculations. Based on the acoustic-electrical analogy method, Qian et al.[10] provided calculation formulas for the composite MPP with various layers. To verify the reliability of the theoretical

Received date: 2025-09-07
Foundation items: National Natural Science Foundation of China (Nos. 51705545 and 15A460041)
* Correspondence should be addressed to LU Yifan, email: 1456869930@qq.com; ZHU Congyun, email: zcy711126@163.com
Citation: Lu Y F, Zhu M K, Zhu C Y, et al. Optimization of multi-layer series micro-perforated panels based on ant colony algorithm[J]. *Journal of Donghua University (English Edition)*, 2026, 43(4): 142-152.

calculation method, they set the initial structural parameters of all-order composite MPPs, and compared them with COMSOL results. However, the study only used graphical visualization to show the model's fitting degree without any quantitative fitting metrics.

When extending to the sound-absorbing structure of multi-layer series MPPs, which involves numerous independent parameters and complex nonlinear mapping relationships, traditional optimization methods are prone to be trapped in local optima. By using a simulated annealing algorithm, Cobo et al. [11] optimized the parameters of three-layer series MPPs, effectively broadened the sound absorption bandwidth and concluded that increasing the number of series layers positively affects its high-frequency sound absorption capability.

This study focuses on the noise frequency range of 100–4 000 Hz. We compare the consistency between the sound absorption coefficients of multi-layer series MPPs calculated by the acoustic-electrical analogy method and the transfer matrix method, as well as their agreement with COMSOL simulation results, as to select the more accurate method. Subsequently, the ant colony algorithm (ACA) is employed to optimize the structural parameters, determining the optimal parameters for series MPPs with various layers under target conditions.

1 Ma's MPP Theory

According to Ma's theory[1-2], a micro-perforated sound-absorbing structure consists of an MPP, a rigid wall, and the air cavity between them. The structural model of MPP is shown in Fig. 1, where d is the pore diameter, t is the panel thickness, and D is the cavity depth.

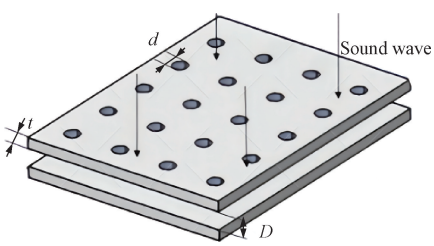


Fig. 1 Structural model of MPP

According to Ma's model, the acoustic impedance Z_S of MPP is

$$Z_S = \rho c(r + j\omega m), \tag{1}$$

where ρ is the air density, and $\rho = 1.226\ \mathrm{kg/m^3}$; c is the speed of sound in air, and $c = 343\ \mathrm{m/s}$; r is the relative acoustic resistance; ω is the angular frequency; m is the relative acoustic mass.

The relative acoustic mass and relative acoustic resistance in Eq. (1) are

$$m = \frac{t}{\theta c}\left[1 + \left(9 + \frac{k^2}{2}\right)^{-0.5} + 0.85\frac{d}{t}\right], \tag{2}$$

$$r = \frac{32\eta t}{\theta \rho c d^2}\left(\sqrt{1 + \frac{k^2}{32}} + \frac{\sqrt{2}}{8}\frac{dk}{t}\right), \tag{3}$$

where θ is the punching rate; η is the viscosity coefficient, with a value of 1.85×10^{-5} Pa·s; k is the perforation constant, and $k = \sqrt{\omega\rho d^2/(4\eta)}$.

The acoustic impedance corresponding to the cavity depth D is Z_D:

$$Z_D = -j\rho c\cot(\omega D/c). \tag{4}$$

2 Reliability of Multi-Layer Series MPP Absorption Calculation Methods

To verify the reliability of the sound absorption coefficient calculations, the sound absorption coefficient curves obtained by both the acoustic-electrical analogy method and the transfer matrix method are compared and analyzed. Their agreement with the results of COMSOL simulations is also assessed.

2.1 Reliability of acoustic-electrical analogy method

Based on the acoustic-electrical analogy method, the acoustic impedance is analogous to the circuit impedance. Therefore, this study uses Ma's single-layer MPP model as the initial theoretical formula and systematically derives the expression for the total acoustic impedance of multi-layer series MPPs based on the equivalent circuit diagrams of the series structure. The total acoustic impedance for multi-layer series MPPs is derived.

2.1.1 Total acoustic impedance of two-layer series MPPs

According to the acoustic-electrical analogy method, the two-layer series MPPs model and its equivalent circuit diagram are shown is Fig. 2.

Based on series-parallel principles, the equivalent circuit is divided into parts, working backward from the final circuit element. The total acoustic impedance of the two-layer series MPPs $Z_{2,\,\mathrm{total}}$ is

$$\begin{cases} Z_{2,1} = Z_{S2,2} + Z_{D2,2}, \\ Z_{2,\,\mathrm{total}} = Z_{S2,1} + 1/(1/Z_{D2,1} + 1/Z_{2,1}), \end{cases} \tag{5}$$

where $Z_{2,1}$ represents the total series impedance of the second-layer MPP and the air cavity; $Z_{S2,1}$ and $Z_{S2,2}$ denote the acoustic impedance of the first-layer MPP and the second-layer MPP, respectively; $Z_{D2,1}$ and $Z_{D2,2}$ correspond to the acoustic impedance of the first air cavity and the second air cavity, respectively.

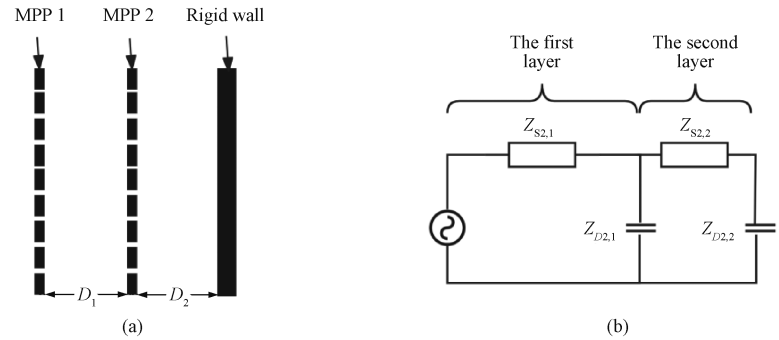


Fig. 2 Two-layer series MPPs and equivalent circuit diagram: (a) structural model; (b) equivalent circuit diagram

2.1.2 Total acoustic impedance of three-layer series MPPs

The three-layer series MPPs model and equivalent circuit diagram are shown in Fig. 3. The total acoustic impedance of the three-layer series MPPs $Z_{3,\text{total}}$ is

$$\begin{cases} Z_{3,1} = Z_{S3,3} + Z_{D3,3}, \\ Z_{3,2} = Z_{S3,2} + 1/(1/Z_{D3,2} + 1/Z_{3,1}), \\ Z_{3,\text{total}} = Z_{S3,1} + 1/(1/Z_{D3,1} + 1/Z_{3,2}), \end{cases} \tag{6}$$

where $Z_{3,1}$ is the total series impedance of the third-layer MPP combined with its air cavities; $Z_{3,2}$ is the total series impedance of the second-layer MPP combined with its air cavity; $Z_{S3,1}$, $Z_{S3,2}$ and $Z_{S3,3}$ are the acoustic impedance of the first-layer to the third-layer MPP, respectively; $Z_{D3,1}$, $Z_{D3,2}$ and $Z_{D3,3}$ are the acoustic impedance of the first to the third air cavities, respectively.

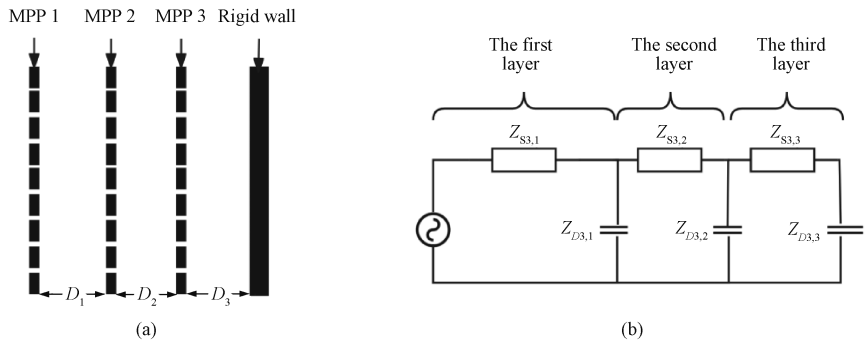


Fig. 3 Three-layer series MPPs and equivalent circuit diagram: (a) structural model; (b) equivalent circuit diagram

2.1.3 Total acoustic impedance of four-layer series MPPs

The four-layer series MPPs model and equivalent circuit diagram are shown in Fig. 4. The total acoustic impedance $Z_{4,\text{total}}$ of the four-layer series MPPs is

$$\begin{cases} Z_{4,1} = Z_{S4,4} + Z_{D4,4}, \\ Z_{4,2} = Z_{S4,3} + 1/(1/Z_{D4,3} + 1/Z_{4,1}), \\ Z_{4,3} = Z_{S4,2} + 1/(1/Z_{D4,2} + 1/Z_{4,2}), \\ Z_{4,\text{total}} = Z_{S4,1} + 1/(1/Z_{D4,1} + 1/Z_{4,3}), \end{cases} \tag{7}$$

where $Z_{4,1}$ is the total series impedance of the fourth-layer MPP combined with its air cavity; $Z_{4,2}$ and $Z_{4,3}$ denote the total series impedance of the third-layer and the second-layer MPP and with their corresponding air cavities, respectively; $Z_{S4,1}$ to $Z_{S4,4}$ correspond to the acoustic impedance of the first-layer to the fourth-layer MPP, respectively; $Z_{D4,1}$ to $Z_{D4,4}$ represent the acoustic impedance of the first to the fourth air cavities, respectively.

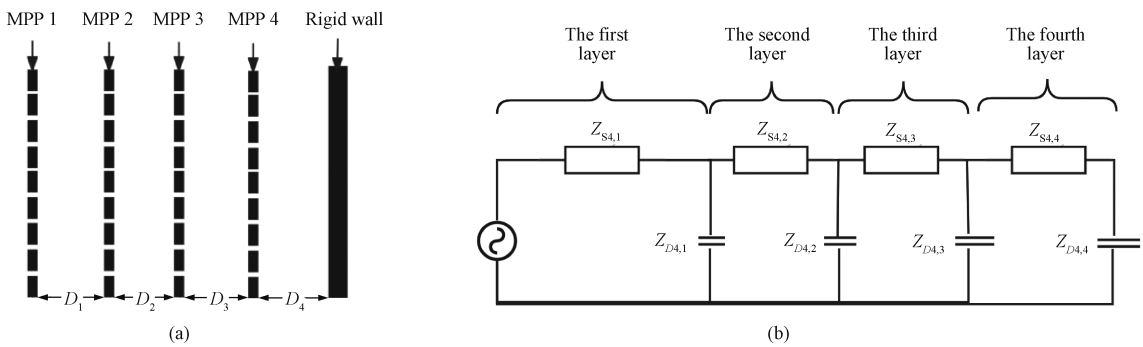


Fig. 4 Four-layer series MPPs and equivalent circuit diagram: (a) structural model; (b) equivalent circuit diagram

2.1.4 Total acoustic impedance of five-layer series MPPs

The five-layer series MPP model and its equivalent circuit diagram are shown in Fig. 5, and the total acoustic impedance $Z_{5,\text{total}}$ of the five-layer series MPPs is

$$\begin{cases} Z_{5,1} = Z_{S5,5} + Z_{D5,5}, \\ Z_{5,2} = Z_{S5,4} + 1/(1/Z_{D5,4} + 1/Z_{5,1}), \\ Z_{5,3} = Z_{S5,3} + 1/(1/Z_{D5,3} + 1/Z_{5,2}), \\ Z_{5,4} = Z_{S5,2} + 1/(1/Z_{D5,2} + 1/Z_{5,3}), \\ Z_{5,\text{total}} = Z_{S5,1} + 1/(1/Z_{D5,1} + 1/Z_{5,4}), \end{cases} \tag{8}$$

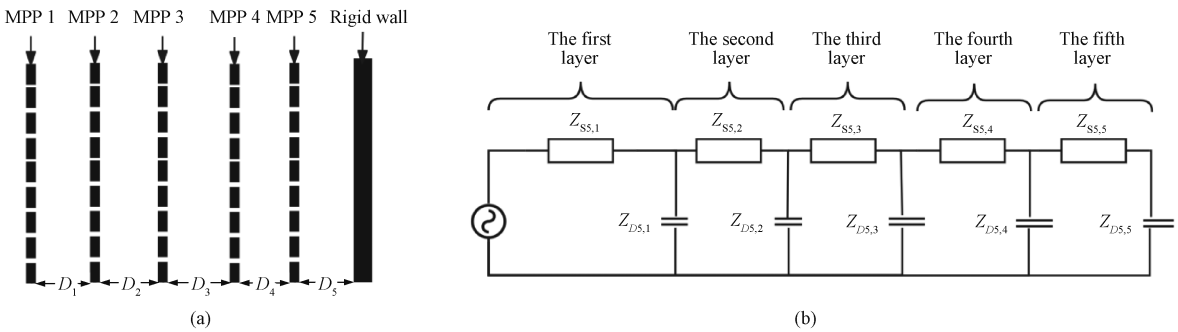


Fig. 5 Five-layer series MPPs and equivalent circuit diagram: (a) structural model; (b) equivalent circuit diagram

where $Z_{5,1}$ is the total series impedance of the fifth-layer MPP combined with its air cavity; $Z_{5,2}$, $Z_{5,3}$ and $Z_{5,4}$ are the total series impedance of the fourth-layer, the third-layer and the second-layer MPPs with their corresponding air cavities, respectively; $Z_{S5,1}$ to $Z_{S5,4}$ correspond to the acoustic impedance of the first-layer to the fifth-layer MPP, respectively; $Z_{D5,1}$ to $Z_{D5,5}$ represent the acoustic impedance of the first to the fifth air cavities, respectively.

2.1.5 Total acoustic impedance of *n*-layer series MPPs

Based on the derivations for above series MPPs and the acoustic-electrical analogy method, the total acoustic impedance rate $Z_{n,\text{total}}$ of n-layer series MPPs is derived. The model and its equivalent circuit are shown in Fig. 6.

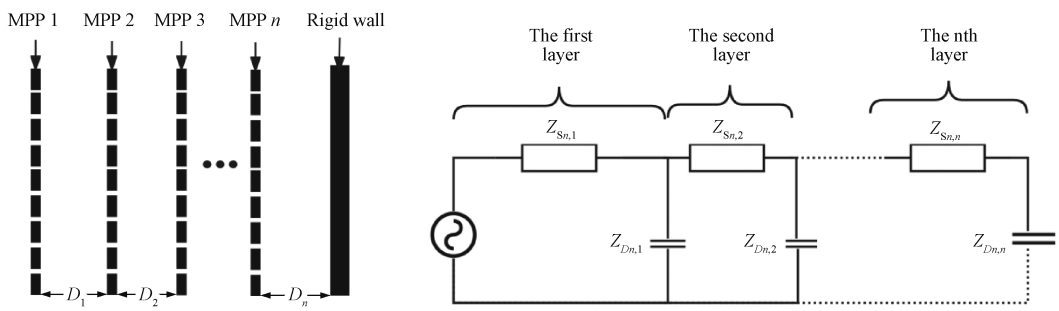


Fig. 6 Basic structure and equivalent circuit diagram of n-layer series MPPs: (a) structural model; (b) equivalent circuit diagram

The total acoustic impedance rate $Z_{n,\text{total}}$ of the n-layer series MPPs is

$$\begin{cases} Z_{n,1} = Z_{Sn,n} + Z_{Dn,n}, \\ Z_{n,i} = Z_{Sn,n+i-1} + 1/(1/Z_{Dn,n+i-1} + 1/Z_{n,i-1}), \\ Z_{n,\text{total}} = Z_{Sn,1} - 1/(1/Z_{Dn,n} + 1/Z_{n,n-1}), \\ \quad i = 2, 3, \cdots, n-1, \end{cases} \tag{9}$$

where $Z_{n,1}$ is the total series impedance of the nth layer MPP combined with its air cavity; $Z_{n,i}$ denotes the total series impedance of the $(n-i+1)$th-layer MPP and its air cavity; $Z_{Sn,1}$ to $Z_{Sn,n}$ correspond to the acoustic impedance of the first-layer to the nth-layer MPP; $Z_{Dn,1}$ to $Z_{Dn,n}$ represent the acoustic impedance of the first to the nth air cavities.

The sound absorption coefficient $\alpha_{e,n}$ is

$$\alpha_{e,n} = \frac{4\text{Re}\left(\dfrac{Z_{n,\text{total}}}{\rho c}\right)}{\left[1 + \text{Re}\left(\dfrac{Z_{n,\text{total}}}{\rho c}\right)\right]^2 + \left[\text{Im}\left(\dfrac{Z_{n,\text{total}}}{\rho c}\right)\right]^2}. \tag{10}$$

2.2 Reliability of transfer matrix method

In this study, the multi-layer structure is decomposed into "panel-cavity" units, and the total transfer matrix and acoustic impedance formula are derived. The transfer matrix method decomposes the n-layer series MPPs into n-layer plates and n cavities, and the surface acoustic impedance is obtained by multiplying the transfer matrices.

In the MPP structure, the transfer matrices consist of two components: $\boldsymbol{S}_i$ for the MPP and $\boldsymbol{H}_i$ for the air cavity,

$i=1, 2, \cdots, n$.

$$\boldsymbol{S}_i = \begin{bmatrix} 1 & Z_{Sn,i} \\ 0 & 1 \end{bmatrix}, \ i = 1, 2, \cdots, n, \tag{11}$$

$$\boldsymbol{H}_i = \begin{bmatrix} \cos(kD_i) & \mathrm{j}\rho c \sin(kD_i) \\ \dfrac{\mathrm{j}\sin(kD_i)}{\rho c} & \cos(kD_i) \end{bmatrix}. \tag{12}$$

By multiplying $\boldsymbol{S}_i$ with $\boldsymbol{H}_i$, the transfer matrix $\boldsymbol{T}$ of the entire structure is obtained:

$$\boldsymbol{T} = \prod_{i=1}^{n} \boldsymbol{S}_i \boldsymbol{H}_i = \begin{bmatrix} T_{11} & T_{12} \\ T_{21} & T_{22} \end{bmatrix}. \tag{13}$$

The total acoustic impedance rate Z_n of the n-layer series MPP structure is

$$Z_n = \frac{T_{11}}{\rho c T_{21}}. \tag{14}$$

Thus, the sound absorption coefficient $\alpha_{t,n}$ of the n-layer series MPPs is

$$\alpha_{t,n} = 1 - \left| \frac{Z_n - \rho c}{Z_n + \rho c} \right|^2. \tag{15}$$

2.3 Comparison of fitting degrees

To compare the consistency of sound absorption coefficients for multi-layer series MPPs calculated by theoretical methods (the acoustic-electrical analogy and transfer matrix methods), COMSOL simulations were performed to obtain the curves. These simulation results were then fitted with the curves obtained from both theoretical methods to assess their consistency.

Finite element models for the multi-layer series MPPs were established in COMSOL as shown in Fig. 7, where a plane wave of 1 Pa was incident in an impedance tube with the MPP positioned at the tube end. Except for the incident surface, all other boundaries were set as rigid walls to achieve total reflection. The MPPs were modeled by COMSOL's built-in perforated plate feature[12].

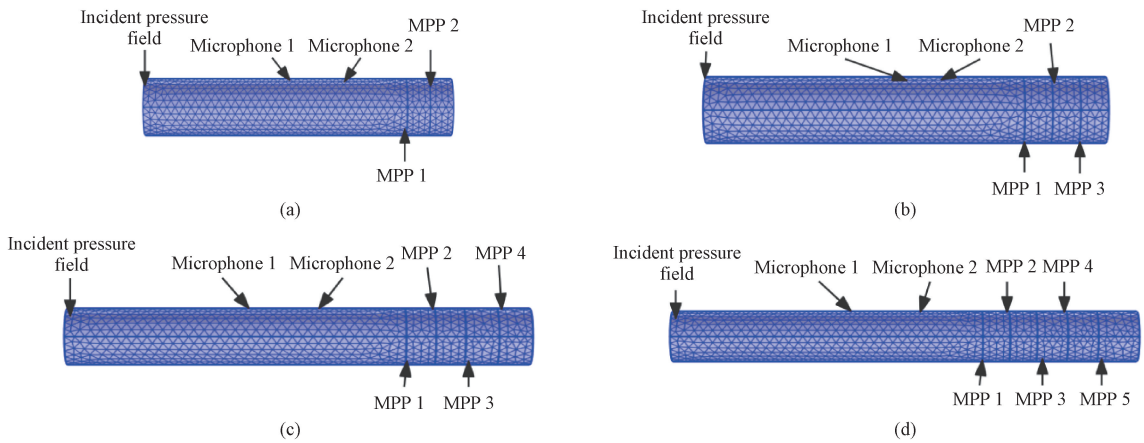


Fig. 7 Finite element models of multi-layer series MPPs: (a) two layers; (b) three layers; (c) four layers; (d) five layers

In the theoretical calculations and simulations, the same structural parameters (Table 1) are used. The root mean square error (RMSE) and coefficient of determination R^2 are compared. The RMSE measures the average error between theoretical values and simulation values, and a lower value indicates a higher fitting accuracy. R^2 ranges between 0 and 1; a larger R^2 signifies higher fitting accuracy, and $R^2=1$ represents perfect fitting[15].

Table 1 Parameters of five-layer series MPP resonator

Position	Pore diameter/mm	Punching rate/%	Panel thickness/mm	Cavity depth/mm
The first layer	0.8	3.0	1.0	40
The second layer	0.8	2.0	1.0	40
The third layer	0.8	1.5	1.0	45
The fourth layer	0.8	2.0	1.0	45
The fifth layer	0.9	0.8	0.5	60

Figures 8 and 9 systematically compare the sound absorption coefficient calculation results between two theoretical methods with COMSOL simulation results.

The transfer matrix method yields lower R^2 and a higher RMSE. The sound absorption coefficient curves generated by the transfer matrix method exhibit a significantly higher degree of consistency with the COMSOL simulation curves.

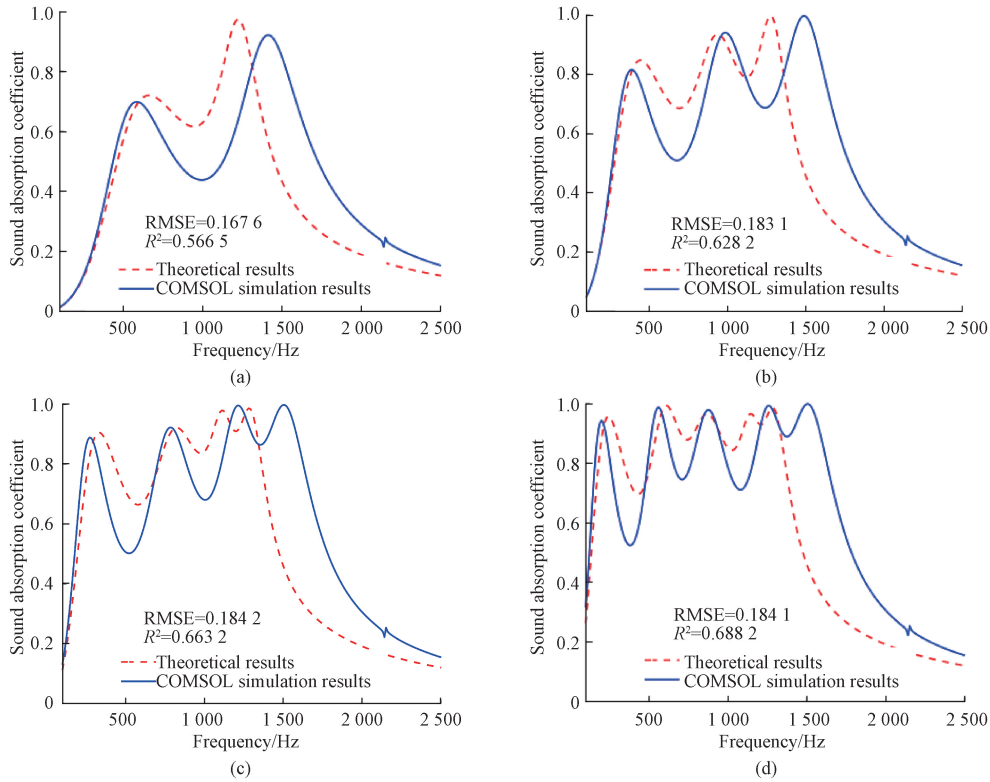


Fig. 8 Comparison of theoretical and simulation curves for multi-layer series MPPs by acoustic-electrical analogy method: (a) two layers; (b) three layers; (c) four layers; (d) five layers

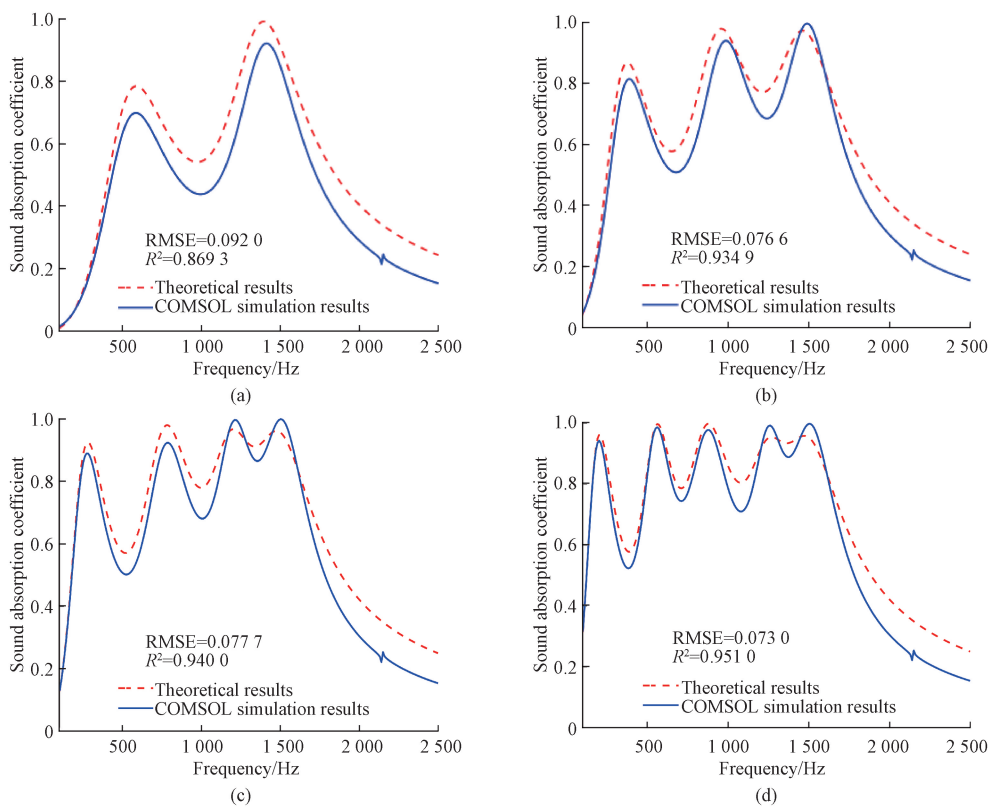


Fig. 9 Comparison of theoretical and simulation curves for multi-layer series MPPs by transfer matrix method: (a) two layers; (b) three layers; (c) four layers; (d) five layers

2.4 Comparison of sound absorption coefficient curves with different layer numbers

To compare the sound absorption performance of MPPs with different layer numbers, numerical simulations were performed in MATLAB based on the transfer matrix method. The structural parameters are listed in Table 1. The resulting sound absorption coefficient curves for series MPPs with different layer numbers are shown in Fig. 10.

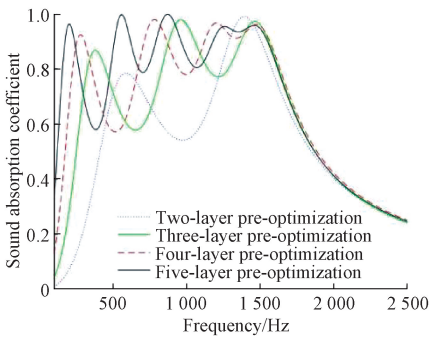


Fig. 10 Sound absorption coefficient curves for series MPPs with different layer numbers

The number of resonant peaks corresponds to the layer numbers of the series MPPs. The five-layer series MPPs exhibit a significantly broader absorption bandwidth compared to the two-layer and three-layer series MPPs, showing substantial overall improvement.

3 Optimization by ACA

3.1 ACA description

To optimize the sound absorption characteristics of multi-layer series MPPs and broaden the effective frequency band, ACA is employed to optimize the parameters. The parameter optimization of multi-layer series MPPs is a typical combinatorial optimization problem, characterized by a large parameter space and strong non-linearity. ACA simulates ant colony foraging behavior and finds the optimal path through a pheromone-driven positive feedback mechanism and collective collaboration[16]. With its strong global search capability, ACA effectively avoids local optima, and is suitable for the optimization objectives of this study. The steps of ACA are as follows[17].

Step 1: an optimization model is established with the objective of maximizing the integrated sound absorption coefficient of the multi-layer series MPP absorber within the specified frequency range. Each ant represents a set of structural parameters, and all parameters to be optimized are sequentially encoded into a vector to generate the initial solution vectors.

Step 2: the transfer matrix method is used to calculate the sound absorption coefficient for each parameter set, which corresponds to the total path length traveled by each ant. Each ant selects the next parameter value based on the pheromone concentration and heuristic information. The state transition probability operator is

$$P_k(\mathrm{iter}) = \frac{\tau_k^{\alpha}(\mathrm{iter}) \cdot \eta_k^{\beta}(\mathrm{iter})}{\sum_{j=1}^{N} \tau_j^{\alpha}(\mathrm{iter}) \cdot \eta_j^{\beta}(\mathrm{iter})}, \tag{16}$$

where P_k is the probability of the kth ant being selected; τ_k is the pheromone concentration for the kth ant; η_k is the heuristic information for the kth ant; α is the importance factor of pheromone; β is the importance factor of heuristic information; N is the total number of ants; iter is the current iteration.

Step 3: based on the value of the integrated sound absorption coefficient, the pheromone concentration is updated accordingly. The pheromone updating operator is

$$\tau_k(\mathrm{iter}+1) = (1-\rho_v) \cdot \tau_k(\mathrm{iter}), \tag{17}$$

$$\tau_{\mathrm{best}}(\mathrm{iter}+1) = \tau_{\mathrm{best}}(\mathrm{iter}) + Q \cdot f_{\mathrm{best}}(\mathrm{iter}), \tag{18}$$

where ρ_v is informational volatility coefficient; Q is the reinforcement coefficient; τ_{best} is pheromone concentration of the global optimal candidate MPP structure at iteration t; f_{best} is the current optimal fitness value.

Step 4: Steps 2 and 3 are repeated until the termination condition is met. At this point, the integrated sound absorption coefficient reaches its maximum, and decoding is performed, i. e., the final solution vector is converted back into the actual MPP parameters.

3.2 Optimal model establishment

In order to quantify the broadband sound absorption performance of multi-layer series MPPs, the value of the sound absorption coefficient in the target frequency band of 100 – 4 000 Hz is set as the optimization target. The mathematical expression of fitness value is obtained by

$$\max(V) = \int_{200}^{4\,000} \alpha(f, d_n, t_n, D_n, \theta_n)\,\mathrm{d}f, \tag{19}$$

where $\max(V)$ is the maximum fitness value.

The parameter ranges are determined based on the actual parameter characteristics of multi-layer series MPPs in the material database, practical manufacturing conditions, application requirements, references to Ma's theory and Ref. [7]. The structural parameters of the multi-layer series MPPs are set as shown in Table 2.

Table 2 Structural parameter setting of multi-layer series MPPs

Parameter	Range
Cavity depth D_n /mm	[0, 80]
Punching rate θ_n /%	[0.5, 5.0]
Panel thickness t_n /mm	[0.1, 1.0]
Pore diameter d_n /mm	[0.3, 1.0]

The parameters of ACA are critical, and the convergence effect depends directly on these parameters[18]. Most of these parameters are determined based on practical experience, and the optimal parameter combinations vary significantly across different problem scales. Therefore, a series of preliminary experiments were conducted to systematically explore reasonable values for parameters: $N = 200$; $m = 500$; $\alpha = 1$; $\rho_v = 0.1$; $\beta = 4$.

3.3 Optimized result comparison between ACA and genetic algorithm

Comparison of sound absorption coefficient curves for five-layer series MPPs optimized by ACA and genetic algorithm is shown in Fig. 11. The average sound absorption coefficient of the five-layer series MPPs optimized by ACA is 0.955. In comparison, the genetic algorithm[19] achieves an average sound absorption coefficient of 0.951. The optimized result by ACA is slightly higher than that by the genetic algorithm.

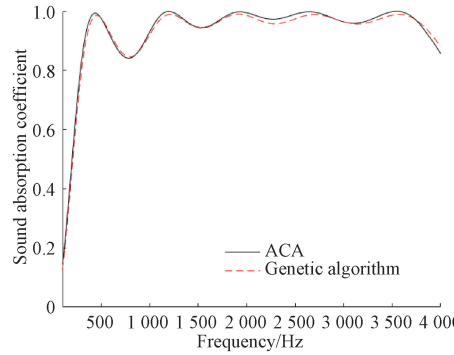


Fig. 11 Sound absorption coefficient curves for five-layer series MPPs optimized by ACA and genetic algorithm

3.4 Optimized results

The solutions with the optimal fitness function value are obtained after independently running ACA 30 times. The optimal structural parameters of multi-layer series MPPs are shown in Table 3.

Table 3 Optimal structural parameters of multi-layer series MPPs

Layer number	Pore diameter/mm	Punching rate/%	Panel thickness/mm	Cavity depth/mm
2	0.300; 0.300	4.784 69; 2.573 23	0.804 41; 0.930 21	13.948 91; 23.832 72
3	0.300; 0.300; 0.300	4.995 80; 4.650 10; 2.480 40	0.564 97; 1.000 00; 1.000 00	14.084 00; 17.810 80; 35.238 60
4	0.300 00; 0.300 00; 0.300 00; 0.300 00	4.591 08; 2.366 52; 1.547 55; 1.000 00	0.280 66; 0.298 77; 0.299 71; 0.299 94	21.385 20; 20.909 53; 24.299 12; 41.867 21
5	0.330 88; 0.300 00; 0.309 48; 0.301 00; 0.321 40	5.002 11; 2.399 08; 1.897 23; 1.190 81; 1.000 72	0.241 72; 0.230 31; 0.266 69; 0.298 89; 0.294 37	22.396 38; 21.132 24; 23.266 96; 29.102 44; 38.535 13

Figure 12 shows a comparison of the sound absorption coefficients before and after optimization for multi-layer series MPPs. In the range of 100–4 000 Hz, the multi-layer series MPPs before optimization perform significantly worse than those after optimization.

Before optimization, the resonant absorption peaks for each series MPPs appear only in the range of 500–1 800 Hz, with anti-resonance frequencies exhibiting absorption coefficients below 0.60. Furthermore, the sound absorption coefficient curves display pronounced fluctuations, and the effective absorption bandwidth is relatively narrow, covering only approximately 200–1 800 Hz.

After optimization, the fluctuations in the sound absorption coefficient curves for the various series MPPs are significantly reduced. The peak values of the resonant absorption peaks within the range of 200–4 000 Hz are all close to 1.00, particularly for the four-layer and five-layer series MPPs. The sound absorption coefficient is greatly improved. The frequency range with a sound absorption coefficient higher than 0.85 expands from 200–1 800 Hz to 200–4 000 Hz. Even at the anti-resonance frequencies (around 880 and 1 000 Hz), the sound absorption coefficient could reach 0.85.

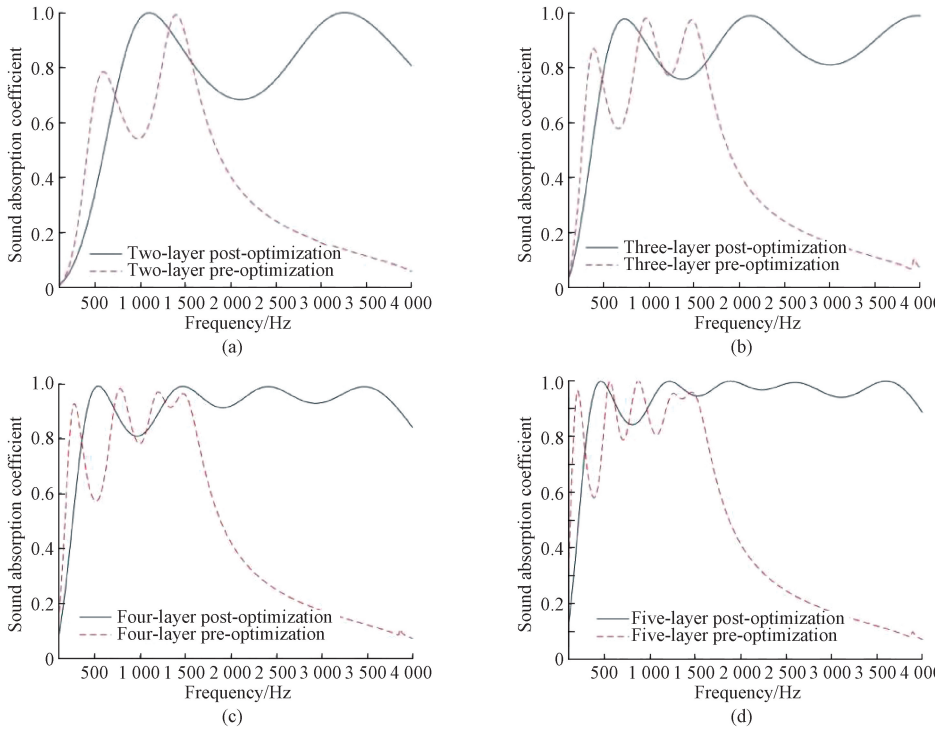


Fig. 12 Sound absorption coefficient curves for multi-layer series MPPs before and after optimization: (a) two layers; (b) three layers; (c) four layers; (d) five layers

3.5 Optimized fitting results

To verify the sensitivity of the optimized results to the theoretical prediction method, the optimized four-layer and five-layer structural parameters in Table 3 were selected for finite element simulation by COMSOL. As shown in Fig. 13, the theoretical predictions based on the transfer matrix method are in excellent agreement with the COMSOL simulation results, with the RMSE lower than 0.08 and R^2 higher than 0.70. This demonstrates that the optimized results are robust.

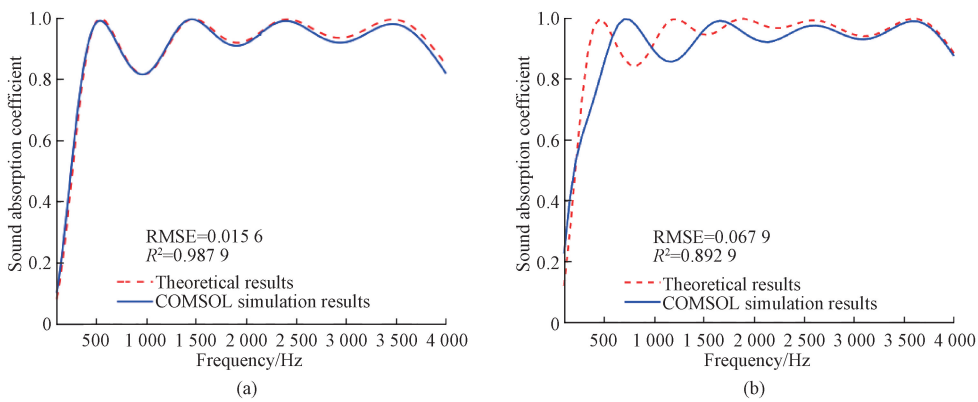


Fig. 13 Optimized fitting results for four-layer and five-layer series MPPs: (a) four layers; (b) five layers

As shown in Fig. 14, the optimized five-layer series MPPs exhibit the broadest absorption bandwidth and the highest absorption coefficient at anti-resonance frequencies. The average sound absorption coefficients for the optimized two-layer, three-layer, and four-layer series MPPs are 0.75, 0.83, 0.93, and 0.96, respectively. Increasing the layer numbers effectively expands the effective absorption bandwidth and improves the average sound absorption coefficient. Therefore, the sound absorption efficiency of multi-layer series MPPs is positively correlated with the layer numbers. However, considering the increased cost, the four-layer series MPPs, which achieve an average sound absorption coefficient of 0.93 in the 100–4 000 Hz frequency band, should be regarded as a more advantageous sound-absorbing structure.

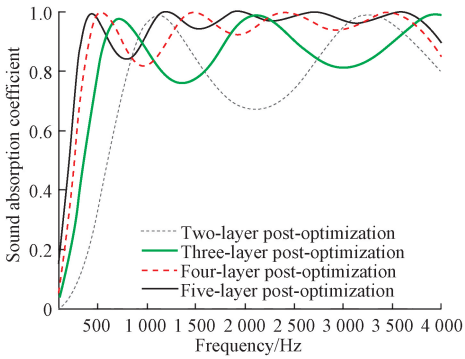


Fig. 14 Comparison of sound absorption performance of multi-layer series MPPs after optimization

4 Conclusions

Based on Ma's theory, the study aims to meet the demand for high-frequency traffic noise control and overcome the bottleneck of the narrow sound absorption bandwidth of a single-layer MPP.

1) The sound absorption coefficient calculated by the transfer matrix method would be more reliable than that obtained by the acoustic-electrical analogy method.

2) The sound absorption performance of the optimized multi-layer series MPPs is comprehensively improved across the range of 100–4 000 Hz. Furthermore, the sound absorption efficiency of multi-layer series MPPs exhibits a positive correlation with the layer numbers. Among the structures studied, the five-layer series MPPs demonstrate the optimal sound absorption performance. The frequency bandwidth with an absorption coefficient higher than 0.85 covers 200–4 000 Hz, and the average absorption coefficient reaches 0.96.

References

[1] Ma D Y. Theory and design of sound absorption structure with micro-perforated plate [J]. *Science in China*, 1975, 5(1): 38-50.

[2] Ma D Y. General theory and design of microperforated-panel absorbers [J]. *Acta Acustica*, 1997, 22(5): 385-393.

[3] Zhang Z M, Gu X T. The theoretical and application study on a double layer microperforated sound absorption structure [J]. *Journal of Sound and Vibration*, 1998, 215(3): 399-405.

[4] Zhang Z M, Fu C J. Unusual photon tunneling in the presence of a layer with a negative refractive index [J]. *Applied Physics Letters*, 2002, 80(6): 1097-1099.

[5] Bravo T, Maury C, Pinhède C. Enhancing sound absorption and transmission through flexible multi-layer micro-perforated structures [J]. *The Journal of the Acoustical Society of America*, 2013, 134(5): 3663-3673.

[6] Zhao X D, Zhao Y Y. Influence of cavity sound mass on double layer micro-perforated panel calculation [J]. *Noise and Vibration Control*, 2008, 28(5): 157-159.

[7] Sheng F, Jiang Z X, He Y Z, et al. Multi-layer micro-perforated panels with broadband absorption for reduction of high-speed railway noise [J]. *Journal of Tongji University (Natural Science)*, 2024, 52(9): 1469-1473. (in Chinese)

[8] Hu J J, Luo G Y. Theoretical analysis and parameter optimization of sound absorption performance of multilayer micro-perforated plate [J]. *Computer & Digital Engineering*, 2024, 52(4): 1235-1246.

[9] Du T, Miao T C, Fu G T, et al. Study on numerical simulation method for the MPP absorber [J]. *Journal of Engineering Thermophysics*, 2015, 36(6): 1242-1246. (in Chinese)

[10] Qian J L, Li G J, Wang R Q, et al. Study on sound absorption characteristics of stepped composite micro-perforated plates [J]. *Noise and Vibration Control*, 2023, 43(4): 262-267. (in Chinese)

[11] Cobo P, De La Colina C, Roibás-millán E, et al. A wideband triple-layer microperforated panel sound absorber [J]. *Composite Structures*, 2019, 226: 111226.

[12] Xing T, Li X H, Gai X L, et al. Simulation technology of sound absorption of micro-perforated panel structures [J]. *Noise and Vibration Control*, 2019, 39(5): 8-11. (in Chinese)

[13] Tang S H, Cai D H, Zhang X B, et al. A composite evaluation method of wavelet denoising with multiplicative combination weights [J]. *Journal of Xiangtan University (Natural Science Edition)*, 2025, 47(2): 168-179. (in Chinese)

[14] Rong M, Feng C, Pang Y P, et al. Research on subway settlement prediction based on WTD-PSR data processing and GSM-SVR model [J]. *Scientific Reports*, 2025, 15(1): 18431-18431.

[15] Hu Q L, He Z H, Zhang S, et al. Statistical evaluation of adsorption kinetic models: goodness of fit and model comparison [J]. *Technology of Water Treatment*, 2025, 51(3): 23-30. (in Chinese)

[16] Wang W T. Research on hybrid ant colony algorithm for some combinatorial optimization problems [D]. Yinchuan: Beifang University of Nationalities, 2023. (in Chinese)

[17] Li J J. Research and application of 3D path planning algorithm based on improved ant colony algorithm [D]. Chengdu: University of

Electronic Science and Technology of China, 2025. (in Chinese)
[18] Yang C X. Path planning of underwater glider based on improved fusion ant colony algorithm [D]. Zhenjiang: Jiangsu University of Science and Technology, 2025. (in Chinese)
[19] Wang Y H, Bo Z W, Liu Z M, et al. On-demand optimization design of composite sound absorber structure [J]. *Machinery Design & Manufacture*, 2023(6): 73-78.

基于蚁群算法的多层串联微穿孔板优化

鲁一帆[1*]，朱梦珂[2]，朱从云[1*]，周冰涛[1]
1. 中原工学院 智能机电工程学院，河南 郑州 450007
2. 南京理工大学 紫金学院，江苏 南京 210046

摘　要：为解决交通高频噪声污染日益突出的问题，针对单层微穿孔板吸声频带较窄的局限性，本研究对多层微穿孔板吸声结构进行了系统研究。首先，基于马大猷微穿孔板理论，分别采用声电类比法和传递矩阵法推导了多层结构的理论吸声模型。其次，通过 COMSOL 仿真对比了两种方法的吸声系数曲线，验证了传递矩阵法在多层结构中的计算优越性。最后，引入蚁群算法对多层串联微穿孔板的结构参数进行优化，以拓展其吸声频带，适应交通高频噪声频段。结果表明，传递矩阵法在预测多层微穿孔板吸声特性方面优于声电类比法，经参数优化后的结构在 100~4 000 Hz 的吸声性能显著提升，且吸声效果随层数的增加而增强。本研究有望为宽频交通噪声控制提供有效的理论依据与设计参考。

关键词：微穿孔板；声电类比法；传递矩阵法；蚁群算法；宽频吸声